DOI 10.5162/Ultrasonic2025/C13-d2

Ultrasonic Imaging for Archaeological Metal Artefacts

Siwei Zhang[1,2], *Ajit Kumar Maddheshiya*[1,3], *Dicky Silitonga*[3], *Pooja Dubey*[1,2], *Phool Singh Yadav*[2], *Raja Ram Yadav*[2], *and Nico F. Declercq*[1,2]

[1] *IRL 2958 Georgia Tech – CNRS, 2 Rue Marconi, 57070 Metz, France*

[2] *George Woodruff School of Mechanical Engineering, Georgia Institute of Technology, Atlanta, GA 30332, United States*

[3] *Department of Physics, Faculty of Science, The University of Allahabad, Prayagraj, Uttar Pradesh 211002, India*

[4] *Arts et Métiers de Metz - LEM3 – UMR CNRS 7239, 4 rue Augustin Fresnel, 57070 Metz, France*

declercq@gatech.edu

Abstract: We assess ultrasound as a noninvasive, low-cost complement for subsurface imaging of metallic archaeological artifacts, addressing the depth limits of optical and spectral methods by applying transmission and reflection modes to minted samples and analyzing peak-to-peak amplitude and time-of-flight. Multiple transducer frequencies and scanning geometries were tested, and reflection-coefficient contrasts confirmed multi-metallic structure. Results show ultrasound's clear potential to extend archaeological analysis at depth.

Keywords: Minted metals, Ultrasound imaging, Archaeology, Surface characterization

Background and Introduction

For over two millennia, minted metals have circulated in commerce and reflect regional cultural–historical dynamics. Beyond their economic role, they serve as archaeological markers, frequently recovered in funerary contexts to help identify tomb owners and periods. Traditional imaging in cultural heritage, such as Hyperspectral Imaging [1] and Polynomial Texture Mapping [2], enhances surface detail but lacks penetration for subsurface characterization. Radiographic methods [3] provide depth but entail high costs and strict radiation controls. This study evaluates ultrasound as a cost-effective, complementary tool for nondestructive subsurface imaging in archaeology. We tested various Euro coins and metallic samples, systematically assessing imaging quality, transducer frequency selection, and feature detection. Higher frequencies improved resolution, and combining transmission and reflection modes enabled estimation of acoustic properties. The results reveal internal structures often missed by conventional imaging and support broader integration of ultrasonics into heritage science, with potential to refine historical interpretation of ancient coins.

Samples

In this study, three samples are investigated: One euro coin (2002) of 2.3 mm thickness with a cupronickel inner core and a nickel-brass outer ring (Figure 1); Two euro coin (2002) of 2.2 mm thickness featuring a nickel-brass center and a copper-nickel outer ring (Figure 2); the trimetallic souvenir badge of 2.2 mm thickness from the Georgia Tech Woodruff School of Mechanical Engineering, showing the steel core with selective nickel, gold, and black nickel (a sulfurized nickel alloy) plating (Figure 2). All of these samples are associated with changes in material properties across different regions, which uncovers the potential for imaging using acoustic characteristics against optical approaches.

Fig. 1: Obv. (left) and rev. (right), 2002 1 Euro coin.

Fig. 2: Obv. views of 2 Euros coin (left) and of trimetallic Georgia Tech souvenir badge (right).

DOI 10.5162/Ultrasonic2025/C13-d2

Experimental setup

Figure 3 shows the experimental setup in transmission configuration with immersion transducer as emitter, needle hydrophone of 0.5 mm diameter as receiver and water-coupled sample coaxially aligned and all immersed in water tank. Samples were steadily held in between the transmitter and the receiver by precision arms of C-Scanner. The samples were positioned such that the hydrophone tip received maximum amplitude along the ultrasonic beam. The scans were obtained by moving the precision arm at the controlled pace while keeping the emitter and receiver fixed. Fixation of samples was first ensured by hot gluing in a preliminary study and further iterated by FDM-printed holders which stabilized the sample and minimized spatial misalignment during scans while facilitating sample replacement in-between. The signal generator, connected to the emitter, produced 2–4 μs pulses in the 1–10 MHz frequency range. The ultrasonic pulse propagated through the medium, interacts with the metal sample, and was captured by the receiving needle. The received signal was then processed and digitized using a high-speed oscilloscope with a fixed sampling rate of 100 MHz. In reflection setup, a single focus-type immersion transducer was used in a pulse-echo configuration. The samples were positioned horizontally on a flat acrylic carrier sheet to ensure that the transducer operated near its focal distance of 10% tolerance to achieve maximum signal strength. The zero reference was taken when the transmitter was in contact with the reference acrylic. During acquisition, the transducer was translated parallel to the sample surface and placed perpendicular to the emission axis. The sample and the transducer were kept immersed in water. A focused-type transducer was selected to eliminate the need for post-processing with beam reconstruction techniques, as suggested in existing literature.([4]). Reflected pulses of 0.1–0.5 μs in the 30–100 MHz frequency range were received and analyzed to identify internal boundaries and qualify surface degradation. No rectification technique was applied, but signal amplification at 12–20 dB was selected depending on the sample surface quality to achieve the clearest results. The pulse-echo reflection setup in Figure 4 was illustrated using a single transducer with water coupling. Care was taken to eliminate air bubbles on the surface of the transducer and the specimen to prevent spurious reflections, and then scanning was carried out in the scan plane formed by the X and Y axes, or respectively scan and index axes as shown in Figure 3 and Figure 4, with resolution determined by incremental step sizes. From optimization of emitter frequency, image quality and data acquisition time, resolution of 0.1 mm was widely applied to most of the scans, except the ones obtained from preliminary study using 0.2 mm resolution (Figures 6a and 6b). Scan speed was selected empirically at 1.2 mm/s for 0.1 mm resolution. A signal averaging count of 180 acquisitions was applied for all scans in both transmission and reflection modes to improve the signal-to-noise ratio.

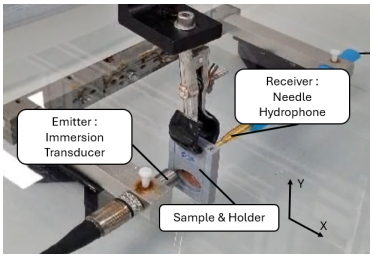

Fig. 3: Transmission-mode Ultrasound Setup.

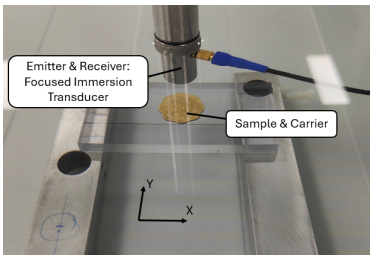

Fig. 4: Reflection-mode Ultrasound Setup.

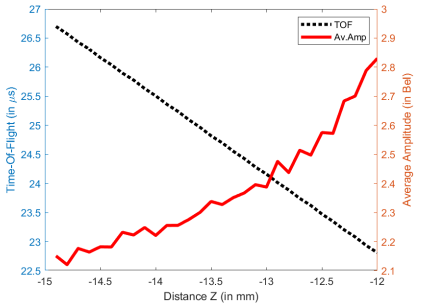

Fig. 5: Graph of variation of peak-to-peak amplitude and time-of-flight averages as a function of distance from focus transducer to reference acrylic in reflection configuration.

Processing method

For each measurement, the maximum peak-to-peak amplitude was extracted from the time-domain signal of each pixel in the C-scan, and the time-of-flight (TOF) was determined as the temporal position corresponding to this maximum amplitude. For transmission mode results, only the amplitude plots are

shown since the TOF plots did not yield significant color contrast revealing coin features. However, an estimation of the speed of sound in metal can be made by measuring sample thickness through calipers and calculating the average TOF over the field region of the sample. For reflection mode results, both the amplitude plots and the TOF plots were obtained and combined to study. The amplitude plots for each of the results are represented on a logarithmic scale to enhance the visualization of signal variations, whereas the TOF value was kept in linear scale. A reference signal from water at the same depth level is obtained to compensate for the effects of acoustic damping in water, the converging nature of the emission beam, and reflections from the acrylic surface. This correction is essential for accurately extracting the longitudinal speed and acoustic impedance of metallic samples using reflection coefficients. As shown in Figure 5, the variation of averaged amplitude and TOF versus distance between the immersion transducer and reference along the vertical Z axis was plotted. The working distance for 100 MHz transducer was fixed at -15 mm, and the samples had a thickness in the range of 1.0-2.5 mm, hence the range of -15 to -12 mm was plotted to calibrate the effects of sample thickness to amplitude. The dashed line in Figure 5 follows a linear trend and its slope corresponds to the longitudinal velocity of 1492 m/s. For a flat transducer with only attenuation in water being considered, the amplitude trend should ideally follow a linear pattern according to the Beer-Lambert law. However, the amplitude profile in the results does not appear to be linear over the entire distance range, due to the focused nature of the transducer. The jagged noise linked to interference artifacts has been reduced by taking an average over 60 pixels, and the averaging is increased until the curve is monotonic and smooth. By averaging amplitude and time-of-flight (TOF) values across the inner and outer ring regions as well as the water background, several (acoustic) properties of the sample can be determined. In reflection mode, TOF plots enable precise estimation of sample thickness. In transmission mode, the longitudinal speed of sound can be derived from TOF measurements. The relative reflection coefficient is obtained by normalizing the amplitude values against a water-based reference, which further allows calculation of the acoustic impedance. Due to the difficulty in decoupling transmission coefficients from attenuation effects in transmission amplitude plots, transmission coefficients were not quantified in this study.

Results

Figures 6a and 6b present the amplitude plots of the 1 Euro sample in transmission mode, highlighting the effects of varying the emitter frequency. It is observed, with an increase in emitter frequency, that the color contrast across different regions was amplified and more pronounced. More relief details with thin thickness and tiny dimension were also revealed at higher frequencies, which can be explained by the interaction of ultrasonic wavelength and the size of design elements. Higher frequency sheds light on more details, but yields stronger attenuation and needs higher amplification. The optimized frequency for the transmission mode is 20 MHz, and the one for the reflection mode is 100 MHz, for instance. The results showing amplitude and TOF of one euro sample are shown in Figure 7a and Figure 7b, respectively. Although the obtained amplitude plots are affected by interference artifacts, they demonstrate higher sensitivity to structural interfaces, clearly revealing the junction in bimetallic regions. In contrast, TOF plots provide clearer representation of overall contrast distribution but exhibit limited sensitivity to fine structural features. Notably, variations in color contrast within the EU territory element are only visible in the amplitude plots, indicating their greater sensitivity to surface roughness. TOF plots, on the other hand, primarily outline the boundaries of different material regions without capturing surface texture. This behavior is consistently observed across other specimens, particularly those with corroded surfaces. The precise thickness of the sample, longitudinal speed of sound, relative reflection or transmission coefficients, absolute coefficients, acoustic impedance and mass density can then be calculated by utilizing both the amplitude and TOF plots in transmission and reflection modes. For the one euro sample in Figure 7a, its field thickness was calculated as 2.25 mm. The relative reflection coefficient of the inner ring with respect to the outer one is 95.1%. For the two euros sample in Figure 8, the field thickness is estimated as 2.14 mm and a relative reflection coefficient of 96.0% is found from the outer region with respect to the inner. The consistency on a slightly higher reflection capability of nickel-brass alloy against copper-nickel

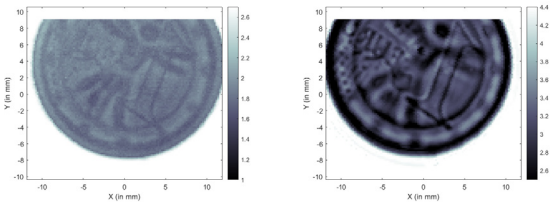

(a) 1 MHz *(b) 5 MHz*

Fig. 6: Transmission amplitude at 1 MHz (left) and 5 MHz (right) for one euro.

alloy is demonstrated by having similar relative reflection coefficient results under a position switch of inner and outer rings in both euro samples. The relative reflection coefficient of black nickel plating with respect to gold plating is 40.4%, which implicitly shows the effects of microstructure and chemical composition on acoustic impedance. One key limitation encountered is the inability to accurately calculate the speed of sound without reliable transmission data, which remains highly susceptible to noise and numerical instability. Similarly, estimating the acoustic impedance requires knowledge of the absolute reflection coefficient, which was not obtained in this study. These challenges highlight the need for improved measurement techniques and calibration strategies. Ongoing efforts are focused on developing refined methods to overcome these issues and enhance the accuracy of ultrasonic property extraction in metallic artifacts.

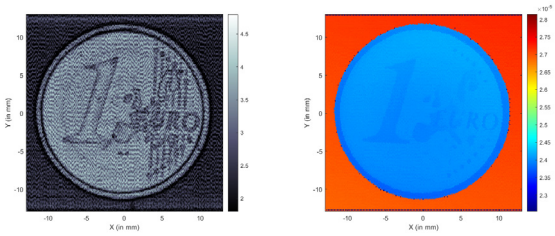

(a) Amplitude (b) TOF

Fig. 7: Reflection amplitude (left) and TOF (right), 100 MHz, 1 euro obv.

Conclusion

The experimental results, as proof-of-concept, demonstrate that both transmission and reflection ultrasound techniques are effective in assessing surface conditions and compositional variations in metallic samples. Higher-frequency emissions enhance spatial resolution, revealing finer details, but are more prone to attenuation. Time-of-flight (TOF) plots in reflection mode enable estimation of local thickness, while

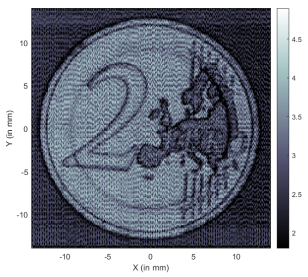

Fig. 8: Reflection amp., 100 MHz, 2 euros obv. face.

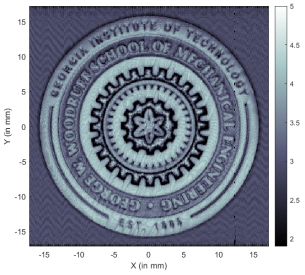

Fig. 9: Reflection amp., 100 MHz, souvenir badge.

amplitude plots provide insights into reflection coefficients and acoustic impedance. In transmission mode, TOF plots allow for calculation of the longitudinal speed of sound, and amplitude plots offer qualitative information on attenuation characteristics. As a low-cost and non-ionizing alternative to X-ray imaging, these approaches provide distinct advantages in detecting acoustic contrasts and material defects which are often invisible under optical inspection alone.

Acknowledgements

Supported by the IMPACT project LUE "I-META," part of the French PIA project "Lorraine Université d'Excellence," reference ANR-15-IDEX-04-LUE.

References

[1] C. Fischer and I. Kakoulli. "Hyperspectral Imaging for Pigment Mapping". In: *Studies in Conservation* 59 (2014), S177–S187. DOI: 10.1179/204705814X13975704318930.

[2] M. Mudge, T. Malzbender, and C. Schroer. "Reflectance Transformation Imaging". In: *VAST: International Symposium on Virtual Reality, Archaeology and Cultural Heritage*. Eurographics. 2006, pp. 145–152.

[3] M. Eveno and A. Duran. "X-ray Tomography of Corroded Coins". In: *Analytical Chemistry* 86.21 (2014), pp. 10849–10855. DOI: 10.1021/ac503075k.

[4] C. W. Yao. "An ultrasonic method for 3D reconstruction of surface topography". In: *Journal of Physics Communications* 2.5 (May 2018), p. 055034. DOI: 10.1088/2399-6528/aac691. URL: https://dx.doi.org/10.1088/2399-6528/aac691.